

# Design of an interdigitated microelectrode biosensor using $\alpha$ -SiC:H surface to capture *E. coli*

José Herrera-Celis<sup>1</sup>, Claudia Reyes-Betanzo<sup>1</sup> and Abdu Orduña-Díaz<sup>2</sup>

<sup>1</sup>Instituto Nacional de Astrofísica, Óptica y Electrónica – Puebla, México

<sup>2</sup>Centro de Investigación en Biotecnología Aplicada del Instituto Politécnico Nacional – Tlaxcala, México

jllhc@inaoep.mx

**Abstract**—This work proposes an interdigitated microelectrode biosensor (IMB), which includes hydrogenated amorphous silicon carbide ( $\alpha$ -SiC:H) as surface to be functionalized. Accordingly, two  $\alpha$ -SiC:H films are included, one on top of SiO<sub>2</sub>, and another on top of microelectrodes. The design along with the medium were simulated on CoventorWare<sup>®</sup> software, taking into account that the IMB proposed will be for the detection of *Escherichia coli*. The influence of both the  $\alpha$ -SiC:H thin film and the capture of bacteria on electrodes on the impedance spectroscopy of the biosensor in the range of 10 kHz to 100 MHz was studied. The results show that the higher the conductivity of the thin film on microelectrodes, the lower is the increase of the magnitude of the impedance spectrum measured in presence of the sterile blank solution, and that the capture of bacteria on microelectrodes increases the sensitivity. The maximum percentage change in the magnitude of impedance of the PIMB is about 45 times greater than that of the conventional interdigitated microelectrode biosensor (CIMB).

**Keywords**—Impedance spectroscopy, interdigitated microelectrode biosensor, hydrogenated amorphous silicon carbide, functionalization.

## I. INTRODUCTION

The interdigitated microelectrode biosensor (IMB) is an electrochemical sensor that has some advantages as its low cost, simplicity of implementation and easy integration in lab-on-chip measurement systems [1-3]. Leaving aside these advantages, there are still aspects of their operation whose understanding could help to increase its sensitivity.

This work presents the design and simulation of an IMB using a functionalized hydrogenated amorphous silicon carbide ( $\alpha$ -SiC:H) thin film as biological receptor. The main idea is to show the effects that the  $\alpha$ -SiC:H thin film on the microelectrodes has in the performance of the biosensor, and how these can be used to capture the analyte on electrodes and increases the sensitivity. Conventional interdigitated microelectrode biosensor (CIMB) uses SiO<sub>2</sub> between electrodes to capture the analyte [4-5]. This configuration reduces the sensing area, which is detrimental for the sensitivity [6]. A functionalized thin film on microelectrodes increases the sensing area, however it could impact the impedance of the blank, reducing the sensitivity. Therefore, not any material could be useful to this purpose.  $\alpha$ -SiC:H has been selected for this function by its biocompatibility and easy doped during deposition [7-10]. Therefore,  $\alpha$ -SiC:H can replace the SiO<sub>2</sub> and has already been used with similar purposes in other types of biosensors [11].

CoventorWare<sup>®</sup> was used to obtain the impedance spectrum in the range of 10 kHz to 100 MHz, simulating the impedance spectroscopy technique by which this type of biosensors is characterized [12-13]. The simulation parameters of the medium were set considering that the biosensor is proposed for the sensing of *Escherichia coli* (*E. coli*), a rod-shaped bacterium that causes severe intestinal and extra-intestinal infections. Humans are infected via gastrointestinal by eating contaminated and bad cooking food, and via urinary by poor health habits [14].

## II. BIOSENSOR DESIGN

### A. Biosensor structure

The proposed interdigitated microelectrode biosensor (PIMB) uses a silicon substrate of 300  $\mu\text{m}$  of thickness, on which is grown 1.5  $\mu\text{m}$  of SiO<sub>2</sub>, and deposited 0.5  $\mu\text{m}$  of undoped  $\alpha$ -SiC:H, 50 nm of titanium and 50 nm of doped  $\alpha$ -SiC:H consecutively. The last two layers are patterned for obtain the array. The finger spacing ( $S$ ) and the finger width ( $W$ ) have been fixed to 5  $\mu\text{m}$  [4-6, 15]. The sensing area is a square of 3.2 mm side length, resulting in 320 interdigitated microelectrodes (ME) of length 3170  $\mu\text{m}$  covering a total sensing area of 10.24 mm<sup>2</sup>. The mean length and diameter of *E. coli* are 2.79  $\mu\text{m}$  and 0.68  $\mu\text{m}$  [16], therefore that sensing area could accommodate around  $5 \times 10^6$  colony-forming unit (CFU).

### B. $\alpha$ -SiC:H and its interaction with the medium

The surfaces of doped and undoped  $\alpha$ -SiC:H films on and between ME, respectively, are functionalized with 3-aminopropyltrimethoxysilane (APTES) in order to obtain amino groups on the surface that contribute to capture bacteria on the biosensor surface. It form a self-assembled monolayer (ML) with a thickness of around of 1 nm. On this layer, by interaction with solution, a double dielectric layer of 5 nm of thickness is formed. Neutral phosphate buffer has been defined as the sterile blank solution and as the medium where the bacteria will be immersed.

### C. The electrical model

Fig. 1 shows the electrical model with bacterial interaction. This model considers the APTES layer, the double dielectric layer and bacteria between ME, also the serial connection of the layers corresponding to APTES, doped  $\alpha$ -SiC:H thin film and double dielectric layer on ME with the parallel connection of the bacteria on ME and the medium on total sensing area.

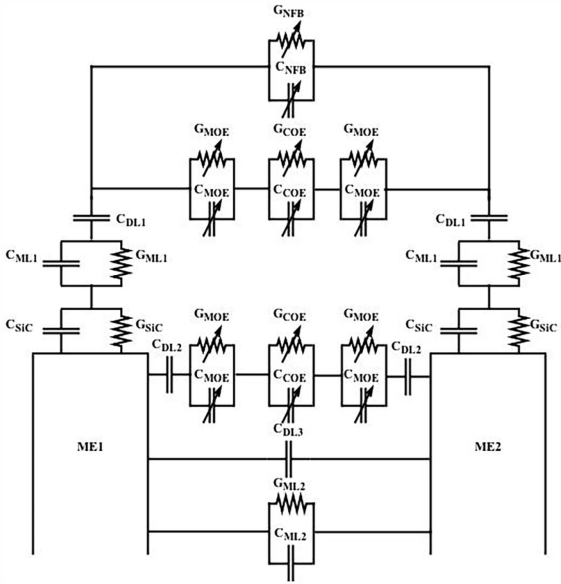


Fig. 1. Electrical model of the biosensor with bacteria on its surface.

Considering the dimensions of the design and the electrical parameters of the APTES layer and the double dielectric layer between ME, these branches can be neglected of the analysis. Some model elements can be neglected inside of the frequency range of this work by their impedance relation with its elements in parallel. For example, the conductances of the membrane of the bacteria on and between ME ( $G_{MOE}$  and  $G_{MBE}$ ) are less than their respective susceptances ( $\omega C_{MOE}$  and  $\omega C_{MBE}$ , where  $\omega$  is the excitation frequency), then  $G_{MOE}$  and  $G_{MBE}$  can be neglected. In other words, the conductivity of the membrane is less than the product  $\omega \epsilon_m$  in the frequency range of this work, where  $\epsilon_m$  is the permittivity of the membrane. In the same way, the susceptances of the cytoplasm of the bacteria on and between ME ( $\omega C_{COE}$  and  $\omega C_{CBE}$ ) in relation to the conductances of the cytoplasm ( $G_{COE}$  and  $G_{CBE}$ ) can be neglected. Bearing in mind the work in [6] and the relative permittivity and conductivity of the neutral phosphate buffer, the susceptance of the medium ( $\omega C_{NFB}$ ) can also be neglected. On the other hand, the susceptances of the APTES layer and the  $\alpha$ -SiC:H thin film on ME ( $\omega C_{ML1}$  and  $\omega C_{SiC}$ ) could be neglected depending on the conductivity of these layers. The simplified electrical model is shown in Fig. 2. Although this model will be used to do any analysis, the elements neglected in it will be included in the simulations.

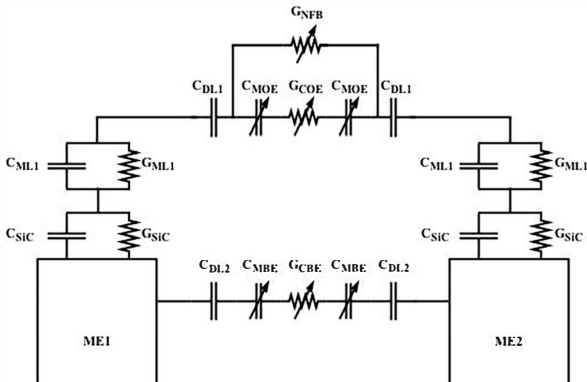


Fig. 2. Simplified electrical model of the biosensor with bacteria on its surface.

The impedance spectrum of the model has three regions. In the first region, the total impedance is predominantly capacitive and dominated by  $C_{DL1}$ . This region extends up to a frequency called low cutoff frequency ( $F_{low}$ ), which the conductance of the medium ( $G_{NFB}$ ) begin to be greater than the susceptance of  $C_{DL1}$ . The second region is predominantly conductive and corresponds to the sum of  $G_{NFB}$ ,  $G_{COE}$  and  $G_{MOE}$  (neglecting  $G_{ML1}$  and  $G_{SiC}$ ). This region extends from  $F_{low}$  to the high cutoff frequency ( $F_{high}$ ), which corresponds to the frequency at which the susceptance of the medium ( $\omega C_{NFB}$ ) achieves to be dominant and begins the third region.

### III. SIMULATION ON COVENTORWARE® SOFTWARE

The CIMP and PIMB structures were built in CoventorWare® software to be simulated using the finite element method. Two vertical planes of symmetry were inserted in the three-dimensional (3D) models to exploit their periodicity and to save computation time. The meshing method selected to create the finite element bricks of the 3D models was Manhattan, while the planes were meshed with surface mesh, with quadrilateral elements. Fig. 3 shows a cross section of two ME with bacteria. The MemElectro solver was used in the electroquasistatic mode. A 1 V sinusoidal signal potential between the terminals of the biosensors with frequency in the range from 10 kHz to 100 MHz was applied.

The electrical parameters of all materials used in simulations are presented in Table I. The APTES thickness was scaled by 50, while the double dielectric layer and the membrane of *E. coli* were scaled by 10. Then, their electrical parameters were also scaled by 50 and 10, respectively, in order to maintain the validity of the results. The titanium thickness was set at 150 nm on models without bacteria and at 200 nm on models with bacteria to minimize the effects of the above scaling. The bacteria was simulated by a rectangular cytoplasm of length 2.5  $\mu\text{m}$  and 0.68  $\mu\text{m}$  of height, extended along the ME and surrounded by the membrane of 50 nm of thickness. The medium thickness was set at 500  $\mu\text{m}$ .

### IV. RESULTS

#### A. Doping level of the $\alpha$ -SiC:H thin film

The variation of the doping level of the  $\alpha$ -SiC:H thin film has been represented in the simulations by a change in conductivity from  $10^{-8}$  S/cm to  $10^{-3}$  S/cm (values reported in [8-10]). Fig. 4 shows the results of the simulations considering medium without bacteria over the PIMB. Hence, it can be seen that the impedance at lower conductivity increases. Given that the sensitivity depends on the change in impedance caused by the capture of bacteria, it will be minimal at low doping level of the film. Then, the conductivity of the  $\alpha$ -SiC:H thin film has been set to  $10^{-3}$  S/cm for the next simulations.

#### B. Capturing position of *E. coli*

Simulations of the 3D PIMB model without and with bacteria covering different areas have been done. Fig. 5 shows that the variation of the magnitude impedance is greater when the bacteria are captured on ME. In addition, bacteria on ME cause a shift in  $F_{low}$  to higher frequencies.

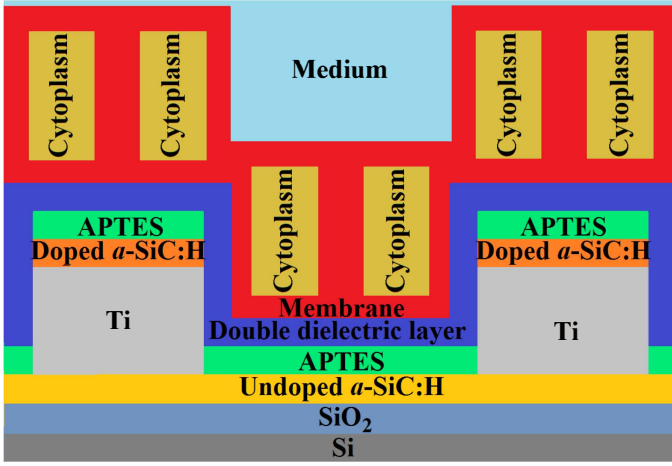


Fig. 3. Cross section of a pair of ME with bacteria on and between them.

TABLE I  
ELECTRICAL PARAMETERS OF MATERIALS, *E. COLI* AND MEDIUM

Material	Conductivity (S/cm)	Relative permittivity
Silicon <sup>a</sup>	$3.33 \times 10^{-1}$	11.9
Silicon dioxide	--	3.9
<i>a</i> -SiC:H undoped <sup>b</sup>	$2.70 \times 10^{-8}$	4.6
Titanium <sup>c</sup>	$2.56 \times 10^4$	--
<i>a</i> -SiC:H doped	from $1 \times 10^{-8}$ to $1 \times 10^{-3}$	4.6
APTES <sup>d</sup>	$5.00 \times 10^{-5}$	2.8
Component of <i>E. coli</i>	Conductivity (S/cm)	Relative permittivity
Membrane <sup>e</sup>	$5.00 \times 10^{-10}$	10
Cytoplasm <sup>e</sup>	$1.70 \times 10^{-3}$	65
Medium	Conductivity (S/cm)	Relative permittivity
Neutral Phosphate Buffer <sup>f</sup>	$9.50 \times 10^{-3}$	80
Double dielectric layer <sup>g</sup>	--	97

<sup>a</sup>Manufacturer data, customer P. O. number 99CE-498/11, Addison Engineering, Inc.

<sup>b</sup>Electric conductivity measured to 300 K within the chamber of the cryostat *Janis Research* maintaining a pressure about of 70 mTorr. Relative permittivity from [7]

<sup>c</sup>Within the range reported in [17]

<sup>d</sup>Within the range reported in [18]

<sup>e</sup>Data from [16]

<sup>f</sup>Manufacturer data, PubChem Substance ID 24888023, Sigma-Aldrich Co.

<sup>g</sup>Data from [6]

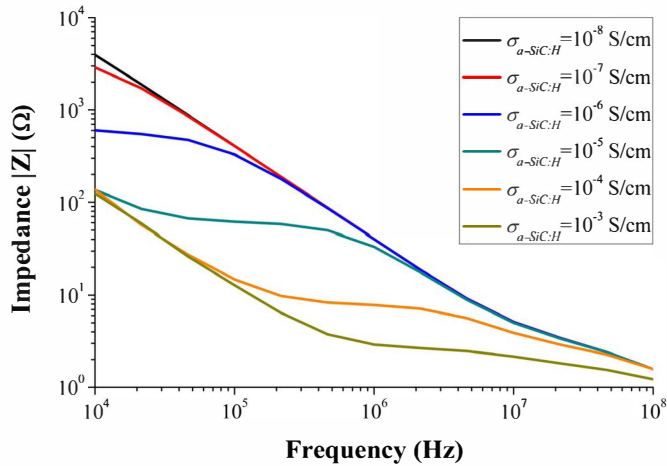


Fig. 4. Simulated electrical impedance of the PIMB with conductivities of the  $a\text{-Si}_{1-x}\text{C}_x\text{H}$  thin film from  $10^{-8}$  S/cm (undoped) to  $10^{-3}$  S/cm (doped).

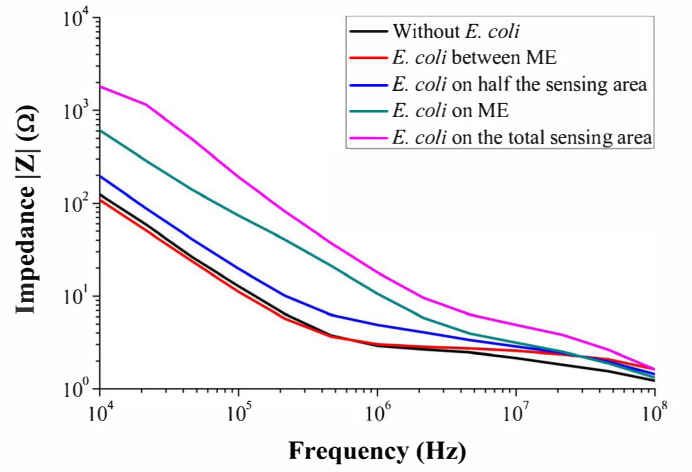


Fig. 5. Simulated response of the PIMB without bacteria and with bacteria covering different areas of the biosensor surface.

### C. Sensitivity analysis

In order to evaluate the gain in sensitivity of the PIMB with respect to the CIMB, simulations have been carried out in each biosensor with both not interaction bacterial and with its maximum area for capture of bacteria. In this regard, it should be noted that the CIMB is designed to capture bacteria only between electrodes, while the maximum capacity of the PIMB is the total area, including the area on ME. Fig. 6 shows that the PIMP has higher sensitivity than the CIMB. This can be evidenced more clearly in Fig. 7, where the spectrum of the percentage change in the impedance magnitude of the PIMB is greater than that of the CIMB, reaching to be 45 times greater around 20 kHz.

## V. DISCUSSION

As more bacteria are captured on ME, less area is occupied by the medium and its equivalent conductance decreases. At the same time, the membrane of *E. coli* reduces the equivalent capacitance because it has less capacitance per unit area than the double dielectric layer. Consequently, the magnitude of the impedance increases and  $F_{low}$  shifts to higher frequencies. It is worth mentioning that the conductivities of the APTES layer and the doped *a*-SiC:H thin film must be within the values used in the simulations in order to improve the sensitivity.

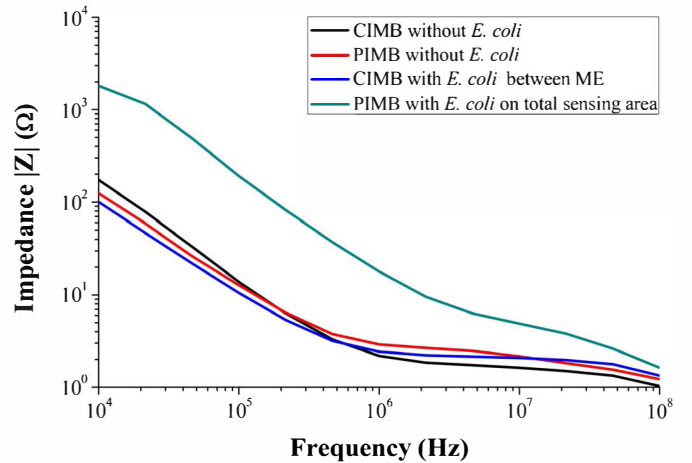


Fig. 6. Simulated impedance spectra of the CIMB and the PIMB without bacteria on their surfaces and with bacteria on the maximum sensing area.

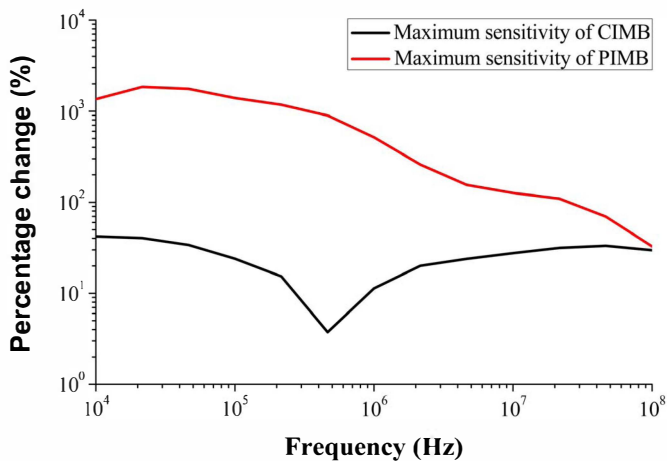


Fig. 7. Maximum percentage change of the impedance spectra.

In contrast, when bacteria are captured between the ME, even though there is an increase in the magnitude of the impedance at frequencies higher than  $F_{low}$  due to the lower conductivity of the cytoplasm relative to the medium, this change is small compared with that observed when bacteria are captured on the ME. One can see that the magnitude of the impedance at frequencies lower than  $F_{low}$  is greater in the simulations without bacteria than in those with bacteria between ME, this is due to a virtual increase of the area on ME, which makes the capacitance  $C_{DLI}$  slightly greater. Then one can conclude that the CIMB has lower sensitivity than the PIMB because the major changes in the impedance spectrum occur when bacteria are captured on the ME.

Experimentally, the CIMBs operate at frequencies lower than  $F_{low}$  because the magnitude of the impedance in this region change with both the capture of bacteria between ME and the change in conductivity of the medium. Instead, the PIMB can operate at frequencies between  $F_{low}$  and  $F_{high}$ , where changes in the magnitude of the impedance are mainly caused by entrapment of bacteria, with a greater sensitivity than the CIMB operating at lower frequencies. Even though sensitivity in this region is not the maximum, the PIMB operating within this region would be less affected by changes in the conductivity of the medium. Furthermore, the sensitivity of the PIMB reaches the maximum value around 20 kHz (below  $F_{low}$ ) when the shift of  $F_{low}$  is maximum.

## VI. CONCLUSIONS

An IMB using  $\alpha$ -SiC:H thin film to capture bacteria on the electrodes, along with bacteria of *E. coli* and their medium were simulated in CoventorWare<sup>®</sup> software. The impedance spectra obtained in the range of 10 kHz to 100 MHz show that if the film has a lower conductivity than  $10^{-3}$  S/cm, the sensitivity of the biosensor is significantly reduced. Also, bacteria captured on the microelectrodes originate a shift of  $F_{low}$ , which can be exploited to sense at lower frequencies, although the thin film is not doped. Finally, the sensitivity of the PIMB is greater because it uses to sense not only the area between microelectrodes but also the area on microelectrodes.

## ACKNOWLEDGMENT

The authors are thankful to Daniela Díaz Alonso by her support with the CoventorWare<sup>®</sup> software and to the National Council of Science and Technology (CONACYT) by financial support with the project No. 242440.

## REFERENCES

- [1] H. Baccar et al, "Interdigitated microelectrode arrays integrated in microfluidic cell for biosensor applications," J. Nanomed. Nanotechnol., vol. 5, pp. 1-4, 2014.
- [2] D. Di et al, "A microelectrode biosensor with Cr/Au quasi-triangle nanodisks for thyroid-stimulating hormone detection," Int. J. Electrochem. Sci., vol. 9, pp. 3618-3627, 2014.
- [3] R. Ohno et al, "Electrochemical impedance spectroscopy biosensor with interdigitated electrode for detection of human immunoglobulin A," Biosens. Bioelectron., vol. 40, pp. 422-426, 2013.
- [4] S. Radke and E. Alócija, "A high density microelectrode array biosensor for detection of *E. coli* O157:H7," Biosens. Bioelectron., vol. 20, pp. 1662-1667, 2005.
- [5] S. Radke and E. Alócija, "Design and fabrication of a microimpedance biosensor for bacterial detection," IEEE Sens. J., vol. 4, pp. 434-440, August 2004.
- [6] M. Ibrahim, J. Claudel, D. Kourtiche and M. Nadi, "Geometric parameters optimization of planar interdigitated electrodes for bioimpedance spectroscopy," J. Electr. Bioimp., vol. 4, pp. 13-22, March 2013.
- [7] S. Sadow, Silicon Carbide Biotechnology: A Biocompatible Semiconductor for Advanced Biomedical Devices and Applications, 1st ed., Elsevier Inc., 2012, pp. 22-28.
- [8] C. Harder, A. Rzany and M. Schaldach, "Coating of vascular stents with antithrombogenic amorphous silicon carbide," Prog. Biomed. Res., pp. 71-77, February 1999.
- [9] F. Demichelis, C. Pirri and E. Tresso, "Influence of doping on the structural and optoelectronic properties of amorphous and microcrystalline silicon carbide," J. Appl. Phys., vol. 72, pp. 1327-1333, August 1992.
- [10] F. Demichelis, C. Pirri, E. Tresso, G. Mea, V. Rigato and P. Rava, "Physical properties of undoped and doped hydrogenated amorphous silicon carbide," Semicond. Sci. Technol., vol. 6, pp. 1141-1146, 1991.
- [11] E. Galopin et al, "Amorphous silicon-carbon alloys for efficient localized surface plasmon resonance sensing," Biosens. Bioelectron., vol. 25, 1199-1203, 2010.
- [12] V. Lvovich, Impedance Spectroscopy: Applications to Electrochemical and Dielectric Phenomena. Hoboken, New Jersey: John Wiley & Sons, Inc., 2012.
- [13] F. Banica, Chemical Sensors and Biosensors: Fundamentals and Applications, 1st ed., John Wiley & Sons, Ltd., 2012, pp. 367-385.
- [14] G. Rodriguez-Angeles, "Diagnosis and main characteristics of *Escherichia coli* pathogenic groups," Salud pública Méx., vol. 44, pp. 464-475, 2002.
- [15] P. Gerwen et al, "Nanoscaled interdigitated electrode arrays for biochemical sensors," Sens. Actuators, B, vol. 49, pp. 73-80, 1998.
- [16] K. Asami, T. Hanai and N. Koizumi, "Dielectric analysis of *Escherichia coli* suspensions in the light of the theory of interfacial polarization," Biophys. J. vol. 31, pp. 215-228, August 1980.
- [17] N. Arsci, J. Lu, C. Lee, J. Yoon, B. Koo and F. Ahmed, "Thickness effect on properties of titanium film deposited by d.c. magnetron sputtering and electron beam evaporation techniques," Bull. Mater. Sci., vol. 36, pp. 807-812, October 2013.
- [18] S. Huang, H. Lee and W. Kang, "Preparation and characterization of proton conductive phosphosilicate membranes based on inorganic-organic hybrid materials," Bull. Korean Chem. Soc., vol. 26, pp. 241-247, 2005.